



## **Molecular structure, spectroscopic assignments and other quantum chemical calculations of anticancer drugs - A review**

A. S. Ghasemi<sup>1</sup>, M. Deilam<sup>1</sup>, J. Sharifi-Rad<sup>2,3,4</sup>, F. Ashrafi<sup>1</sup> and S. M. Hoseini-Alfatemi<sup>4</sup>

<sup>1</sup>Department of Chemistry, Payame Noor University, P.O. Box, 19395-3697 Tehran, Iran

<sup>2</sup>Zabol Medicinal Plants Research Center, Zabol University of Medical Sciences, Zabol, Iran

<sup>3</sup>Department of Pharmacognosy, Faculty of Pharmacy, Zabol University of Medical Sciences, Zabol, Iran

<sup>4</sup>Pediatric Infections Research Center, Mofid Children Hospital, Shahid Beheshti University of Medical Sciences, Tehran, Iran

**Corresponding author:** Javad Sharifi-Rad, Zabol Medicinal Plants Research Center, Zabol University of Medical Sciences, Zabol 61615-585, Iran. Email: [javad.sharifrad@gmail.com](mailto:javad.sharifrad@gmail.com)

### **Abstract**

In many texts, both theoretical and experimental studies on molecular structure and spectroscopic assignments of anticancer medicines have been reported. Molecular geometry parameters have been experimentally obtained by x-ray structure determination method and optimized using computational chemistry method like density functional theory. In this review, we consider calculations based on density function theory at B3LYP/6-31G (d,p) and B3LYP/6-311++G (d,p) levels of theory. Based on optimized geometric parameters of the molecules, molecular structures (length of bonds, bond angles and torsion angles) and vibrational assignments have been obtained. Molecular stability and bond strength have been investigated by applying natural bond orbital (NBO) analysis. Other molecular properties such as Mulliken population analysis, thermodynamic properties and polarizabilities of these drugs have been reported. Calculated energies of HOMO and LUMO show that charge transfer occurs in the molecular. Information about the size, shape, charge density distribution and site of molecular chemical reactivity has been obtained by mapping electron density isosurface of electrostatic and compared with experiment data.

**Key words:** Anticancer drugs, density functional theory, molecular structure, vibrational assignments.

### **Introduction**

A malignant cancer grows unrestricted and progressively invades the vital organs of the body, thus participating to malignancy. The failure of chemotherapy used in cancer treatment can be due to the phenomenon of multidrug resistance in cancer cells (1-3). In addition X-ray therapy and chemotherapy are used in most cases despite having side effects which are created by drug's being non specific and highly toxic. Many antineoplastic agents used in clinical such as alkylating agents, antimetabolites, nitrosoureas, plant alkaloids, antibiotics, enzymes, hormones and radioactive isotopes. These agents are chemically different compounds with different modes of actions (4). Researchers use X-ray, neutron and electron diffractions to determine molecular structure of a compounds. Although each of the methods have different advantages toward each other, today the most commonly used method is X-ray diffraction. This method is used to determined molecular geometry from organic compounds to metal complexes with high accuracy. In order to support experimental data, quantum chemical computational methods are applied. This is a transparent fact that density functional theory (DFT) has been the most common method in computational chemistry for the past 10 years (5). In many studies, DFT is used for study the interaction of CNCl molecule with the pristine; Al-, Ga-doped BN nanotubes (6). DFT calculation is used for investigating adsorption properties of single-walled carbon nanotube as a gas sensor and optimizing adsorption for CO adsorptions, O<sub>2</sub> and N<sub>2</sub> adsorptions in computational NMR and NQR study (7-20). In order to understand the biological and anticancer

activity of some medicines, it is inevitable to study the physicochemical properties of anticancer drugs alone or anticancer drugs carrier conjugates. Therefore researchers have used density functional theory calculations (21-32). In this review, we explain density functional theory method which was carried out on some anticancer drugs, comparing them with experimental data.

### **Materials and methods**

The aim of each quantum chemical method is to find computation solutions to the time independent schrodinger equation (TISE), providing electronic energies, electron densities and properties related to wavefunction of the system for a given molecular geometry and an electronic configuration. Thus TISE is a multidimensional matter which cannot be solved exactly. Therefore, different approximations or "models", each with different accuracy and applicability, have been developed in the last decades. Most of these approximations are divided into two big groups named ab-initio and density theory function (DFT), depending on electronic wavefunction or electronic density, respectively (33). DFT is different from wavefunction theory namely it uses electron density as a main variable (34-40). All ground state features of the molecule are determined by the ground state density while the time-dependent DFT (TD-DFT) method allows us to do calculations of excited state features (38,41,42). Kohn-sham DFT; the most widely used DFT for molecules, uses a molecular orbital formalism like the wavefunction theory and kohn-sham equations, which are the same as HF equations, having exchange-correlation functionals-analytical expressions

**Table 1.** Optimized geometric parameters at the B3LYP/6-31G (d,p) level of theory for DMBC (41).

Bond Lengths (Å)			Bond Angles (°)			Dihedral Angles (°)		
Parameter	6-31G (d,p)	X-Ray	Parameter	6-31G (d,p)	X-Ray	Parameter	6-31G (d,p)	X-Ray
C1 C2	1.385	1.377	C1C2C3	121.2	120.7	C1C2C3C4	0.08	0.05
C2 C3	1.415	1.409	C2C3C4	118.2	118.5	C2C3C4C5	0.16	-0.4
C3 C4	1.399	1.387	C3C4C5	121.2	121.7	C3C4C5C6	0.11	1.4
C4 C5	1.396	1.402	C4C5C6	120.3	119.1	C3C2C1O7	179.8	178.9
C5 C6	1.393	1.389	C2C1O7	125.2	125.4	C2C1O7C8	0.4	0.0
C1 O7	1.360	1.367	C1O7C8	118.0	116.3	C1O7C8H9	179.5	176.8
O7 C8	1.418	1.427	O7C8 H 9	105.9	109.4	C1O7C8H10	60.7	63.1
C8 H 9	1.090	0.960	O7 C8 H 10	111.6	109.4	C1O7C8H11	61.6	56.8
C8 H10	1.097	0.960	O7 C8H11	111.6	109.4	O7C1C2H12	0.0	0.9
C8 H 11	1.097	0.960	C1C2H 12	119.4	119.6	C2C3C4H13	179.8	179.5
C2 H 12	1.082	0.930	C3C4H 13	119.4	119.2	C3C4C5H14	179.9	178.5
C4 H 13	1.085	0.930	C4C5H 14	119.4	120.3	C4C5C6O15	179.9	179.0
C5 H 14	1.083	0.930	C5C6O15	125.2	125.0	C5C6O15C16	0.03	-4.0
C6 O 15	1.355	1.361	C6O15C16	118.1	117.3	C6O15C16H17	179.9	178.5
O15 C16	1.420	1.436	O15C16H17	105.8	109.5	C6O15C16H18	61.1	58.5
C16 H 17	1.090	0.960	O15C16H18	111.5	109.4	C6O15C16H19	61.2	61.4
C16 H 18	1.097	0.960	O15C16H19	111.5	109.4	C1C2C3C20	179.9	-178.7
C16 H 19	1.097	0.960	C2C3C20	123.0	122.3	C2C3C20H21	178.2	-173.1
C3 C20	1.454	1.461	C2C3 H21	115.8	116.6	C2C3C20C22	1.8	6.9
C20 H 21	1.089	0.930	C2C3C22	128.4	126.6	C3C20C22H23	0.4	-0.9
C20 C22	1.351	1.339	C20C22H23	121.1	119.0	C3C20C22C24	179.1	179.0
C22 H 23	1.084	0.929	C20C22C24	120.0	121.9	C20C22C24O25	4.5	-7.6
C22 C24	1.477	1.476	C22C24O25	121.6	121.6	C20C22C24C26	176.2	171.4
C24 O25	1.231	1.226	C22C24C26	119.1	118.6	C22C24C26C27	13.6	-3.0
C24 C26	1.504	1.503	C24C26C27	123.9	122.9	C24C26C27C28	179.0	-177.5
C26 C27	1.402	1.395	C26C27C28	120.9	121.1	C26C27C28C29	0.3	0.4
C27 C28	1.394	1.385	C27C28C29	119.0	119.8	C27C28C29C30	0.5	-2.0
C28 C29	1.392	1.379	C28C29C30	121.2	121.7	C28C29C30C31	0.09	2.0
C29 C30	1.395	1.388	C29C30C31	118.9	118.6	C24C26C27H32	0.49	2.55
C30 C31	1.390	1.382	C26C27H32	120.7	119.3	C26C27C28H33	179.4	-179.5
C27 H32	1.084	0.931	C27C28H33	120.7	120.5	C28C29C30H34	179.7	-178.0
C28 H33	1.083	0.929	C29C30H34	120.1	120.6	C29C30C31H35	179.3	179.8
C30 H34	1.083	0.931	C30C31H35	120.8	119.3	C27C28C29Br36	179.5	176.8
C31 H35	1.084	0.929	C28C29Br36	119.3	118.8	-	-	-
C29 Br36	1.910	1.908	-	-	-	-	-	-

dependent on the electron density which describe electron exchange and correlation. This matter let us have calculations at a computational cost comparable to HF, while having electron correlation is unknown. Instead, there is a large number of approximate exchange-correlation functionals which use different approximations, leading to different suitability for different applications and chemical problems (33).

## Discussion

### Molecular structure

Researchers have down a series of DFT calculations on anticancer drugs using both the B3LYP/6-311++G (d,p) and 6-31G (d,p) methods. The first part of computational studies is determination of molecular geometry. These have found optimized molecular structures of drugs. For example, the optimized molecular structures of the DBHQ and DCHQ belonging to C1 point group symmetry have been obtained. The optimized bond length and bond angles of the DBHQ and DCHQ are computeded, using DFT (B3LYP) method with 6-311++G basis set. The optimized structures of these molecules were compared with other similar systems for which the crystal structures have been solved. Based on theoretical values, we find out that most of the optimized bond lengths and bond angles are slightly longer or shorter than experimental values. The obtained bond angles and bond lengths of DBHQ and DCHQ molecules at B3LYP/6-311++G (d,p) method have created geometrical parameters which are much closer to experimental values (43). The organic molecules, MEP especially chalcone derivatives, constitute a significant group of natural products and some of them have a wide range

of biological activities such as anticancer. Structural studies on chalcone derivative 1-(4-Bromophenyl)-3(3,4-dimethoxy-phenyl) prop-2-en-1-one (DMBC) have recently been reported. optimized structural parameters of DMBC calculated using B3LYP/6-31G (d,p) basis set were obtained and listed in Table 1 along with experimental data, according to atom numbering scheme in Figure 1. The agreement between experimental and optimized crystal structure is quite good, showing the geometry optimization often reproduces exactly experimental conformation (44). Also for the other anticancer drugs like rosmarinic acid, the most important structural parameters, such as bond lengths, bond angles and dihedral angles have been determined by density functional theoretical calculations with 6-31G (d,p) basis set. Geometry optimizations were down without any symmetry constraint; including polarization function to correctly take into account intramolecular H-bonding in the molecule (45). Mitotane also known as o,p'-DDD, is an anti-neoplastic drug used for the treatment of adrenocortical carcinoma, it is an isomer of DDD and a derivative of di-

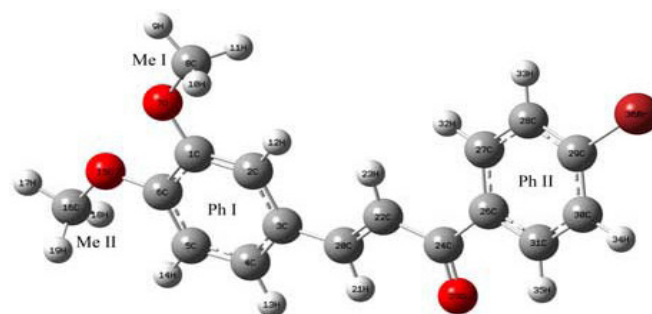


**Figure 1.** Atomic numbering and molecular structure of DMBC (44).

chloro diphenyl trichloroethane (DDT). The optimized geometries of mitotane and DDD structures have been determined at B3LYP/6-311++G (d,p) level of theory (46). Flavonoids are a large group of herbal compounds that diversity from their structure causes antineoplastic and antioxidant activities to be made (47). The molecular properties of these compounds have been calculated by B3LYP/6-311G (d,p) (48). 2-TH and its derivatives have been used in a wide range of applications specially as anticarcinogenic. All calculations on 2-thioxo analogues were done at the B3LYP/6-311++G (d,p) theory (49). Also a new ethyl 4-formyl-3,5-dimethyl-1H-pyrrole-2-carboxylate thiosemicarbazone (EFDMPCT) has been synthesized and characterized by quantum chemical calculations with DFT and using B3LYP/6-31G(d,p) level of theory (50).

### Vibrational assignments

The assignment of experimental wavenumber is not an easy task and in this respect, calculation of vibrational wavenumbers is a good target for spectra assignment. The analysis of the vibrational spectra is based on experimental FT-IR spectrum, FT-Raman spectrum and vibrational spectra calculated by their scaled wavenumbers. The majority of observed vibrational modes are coinciding in both IR and Raman spectra. The obtained vibrational frequency by DFT calculation is well-

known for overestimation from experimental values by 2-7 % on average. An effort was made to refine the scale factors, using the set of transferable scale factors which are recommended by Pulay *et al.* (51). Vibrational frequencies calculated on B3LYP/6-311++G (d,p) level were scaled by 0.8821 for wavenumbers less than 1700  $\text{cm}^{-1}$  at 0.9811 for higher than that. The vibrational assignments for DBHQ and DCHQ are based on DFT/6-311++G (d,p) frequencies, Infrared intensities, Raman activities as well as particular group frequencies. The 48 normal states of DBHQ and DCHQ are distributed among the symmetry types as 19 stretching, 14 in-plane bending and 15 out-of-plane bending states (43). The analysis of detailed vibrational spectrum for DMBC was done based on the normal coordinate analysis according to the scaled quantum mechanical force field method. The distribution of potential energy reveals that many of internal modes contribute to a particular vibrational mode and include simultaneous motion of a large number of atoms. The observed and calculated wavenumbers along with infrared and Raman intensities are listed in Table 2. A comparison of observed and calculated IR and FT-Raman spectra of DMBC has been presented in Figures 2 and 3 which helps to find out observed spectral features. The calculated spectrum was found to be close to experimental data and was reasonable in terms of accuracy. H-atoms engaged with

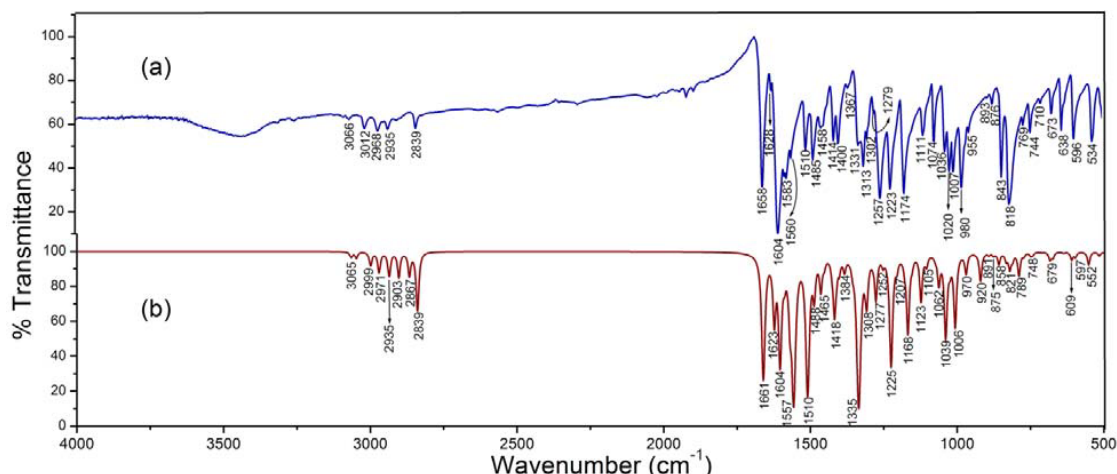


**Figure 2.** (a) Experimental FT-IR spectra in the range 4000–400  $\text{cm}^{-1}$  and (b) Simulated IR spectra by B3LYP/6-31G (d,p) level of theory for DMBC (44).

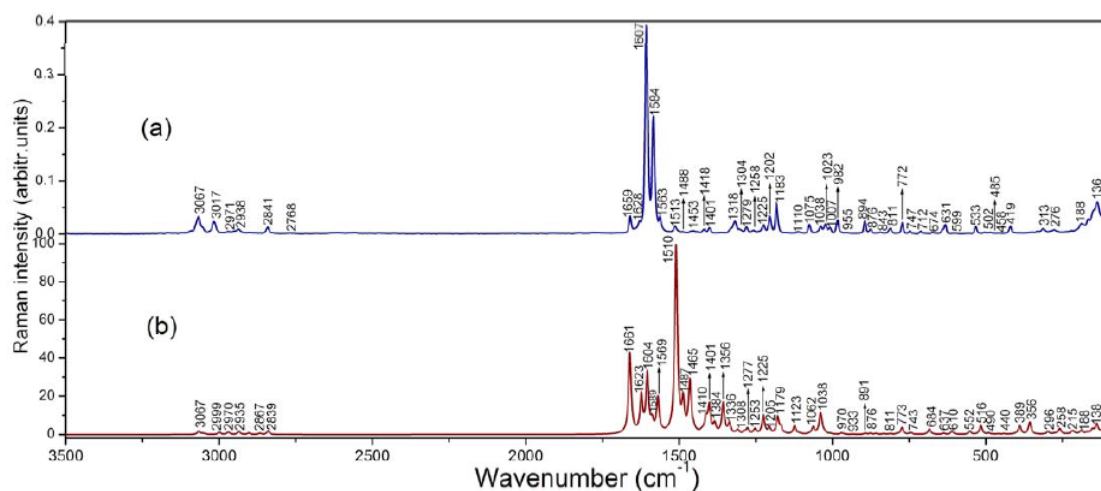


**Figure 3.** (a) Experimental FT-Raman spectra in the range 3500–50  $\text{cm}^{-1}$  (b) Simulated Raman spectra at the B3LYP/6-31G (d,p) level of theory for DMBC (44).

**Table 2.** Comparison between calculated and observed wavenumbers for DMBC (44).

Calculated wavenumbers (cm <sup>-1</sup> )		Observed wavenumbers (cm <sup>-1</sup> )		IR Intensity	Raman Intensity
Unscaled	Scaled	FTIR	Raman		
3232	3067	3066vw	3067w	3.51	11
3228	3064	-	-	3.56	2.79
3014	2839	2839 w	2841vw	88.91	6.93
1736	1661	1658 vs	1659 w	340.69	339
1662	1623	1628 vw	1628 vw	126.04	154
1642	1604	1604 vs	1607 vs	269.67	248
1637	1588	1583 w	1584 s	25.03	42.5
1622	1569	-	1563 w	109.90	144
1614	1557	1560 w	-	550.75	2.73
1306	1277	1279 vw	1279 w	75.76	22.2
1276	1253	1257 vs	-	12.82	19.3
1233	1225	1223 vs	1225 w	275.63	78.6
1226	1205	-	1202 w	17.47	25.7

intermolecular H-bonds increase deviations of the simulated spectra from the experimental spectra showing the theoretical spectrum was obtained in gas phase without considering intermolecular H-bonding effects (44). The molecular structure of rosmarinic acid is made up of 42 atoms; so this molecule has 120 normal modes of vibration. The molecular conformation yielded by geometry optimization shows no special symmetries thus the molecule belongs to C<sub>1</sub> point group. As a result all the 120 fundamental vibrations of the free molecule are active in both IR and Raman spectra. Assigned wavenumbers of all vibrational modes have been computed at B3LYP level with the basis set 6-31G (d,p). Researchers have pursued scaling factor of 0.9608 for B3LYP/6-31G (d,p). After scaling with scaling factor, deviation from experimental modes was less than 10 cm<sup>-1</sup> with few exceptions. Comparing calculated frequencies reveals the result of 6-31G (d,p) basis set has very good agreement with experimental observations, even for complicated molecular system (45). Mitotane belongs to C<sub>1</sub> point group symmetry. In order to consider the performance and vibrational wavenumbers for Mitotane root mean square (RMS) value and correlation coefficient between calculated harmonic  $\nu$ (cal) and experimental  $\nu$ (exp) vibrational wavenumbers for each molecule were calculated by 6-311++G (d,p) basis set. RMS values of wavenumbers was calculated from

$$RMS = \sqrt{\frac{1}{n-1} \sum_i^n (v_i^{\text{calc}} - v_i^{\text{exp}})^2} \quad (3)$$

Where 'n' is the number of observed or calculated data. The RMS error of the unscaled and experimental wavenumbers was found to be 52.8 cm<sup>-1</sup> and 66.3 cm<sup>-1</sup> for IR and Raman wavenumbers, respectively. For reproducing the observed wavenumbers, the scaled factors were refined and optimized via a least squares refinement algorithm which resulted in RMS deviation of a 8.5 cm<sup>-1</sup> and 10.2 cm<sup>-1</sup>, respectively between experimental and scaled quantum mechanical wavenumbers. Based on these results, we can get conclusion that scaled wavenumbers are closely reproduced the observed fundamentals. As we said about DMBC, it must be because of this fact that exiting Hydrogen bond vibrations in the crystal lead to strong perturbation of the infrared wavenumbers and intensities of many other modes. Also, we express that experimental and theoretical calculations results belong to solid and gaseous phase, respectively (46).

### Natural Bond Orbital analysis

Natural bond orbital (NBO) analysis provides an efficient method to study interactions in both filled and virtual orbital spaces which cause the analysis of intra and inter molecular interactions to be enhanced. NBO computations have been done at DFT method which presents information about intra molecular hydrogen bonding, delocalization of electron density and intra molecular charge transfer (ICT) within the molecule. The second order perturbation theory analysis of Fock matrix in NBO basis indicates strong intra molecular hyper conjugative interactions of  $\pi$  electrons. The larger values of  $E(2)$ , the more intensive the interaction between electron donors and electron acceptors and the greater rate of conjugation of the whole system. The hyperconjugative interaction energy resulted from the second order perturbation approach is

$$E(2) = -n_{\sigma} \frac{\langle \sigma | F | \sigma \rangle^2}{\epsilon_{\sigma}^* - \epsilon_{\sigma}} = -n_{\sigma} \frac{F_{ij}^2}{\Delta E} \quad (5)$$

Where  $n_{\sigma}$  is the populations of the donor  $\sigma$  orbital,  $\langle \sigma | F | \sigma \rangle^2$  or  $F_{ij}^2$  is the Fock matrix element of the  $i$  and  $j$  NBO orbitals and  $\epsilon_{\sigma}$  and  $\epsilon_{\sigma}^*$  are the energies of  $\sigma$  and NBOs (44). Lately, it has been found that C-H group can be a hydrogen-bond donor. Although C-H...O interactions are considered weak; these are the second most important group while forming 20-25 % of the total numbers of hydrogen bonds. These interactions have been proven to be of greater significance in biological systems in order to clear the relationship of the structure activity. The result of NBO in rosmarinic acid reflects the charge transfer mostly due to O-H and COOH group. The NBO analysis showed that  $\pi \rightarrow \pi^*$  interaction offers the strongest stabilizations to the systems (45). The stabilization energy for DBHQ and DCHQ has been computed from the second order perturbation theory. The calculated equilibrium geometries indicate changes in the neighborhood of bromine and chlorine atoms. The NBO analysis proves differences in interaction energies are because of the substitutions of electronegative atoms like N, Br and Cl, respectively (43). In DMBC molecule, the strong intra molecular hyper conjugative interaction of  $\pi$  and  $\pi$  electron of C-C bond with C-C anti bond of both the Phenyl rings result in stabilization of the system. The charge transfer happening within the molecule is more in  $\pi \rightarrow \pi^*$  transition. The intra molecular C-H...O hydrogen bond

**Table 3.** Second order perturbation theory analysis of fock matrix in NBO basis at the B3LYP/6-31G (d,p) level of theory of DMBC (44).

Donor (i)	ED (i) (e)	Acceptor (j)	ED (j) (e)	$E(2)^a$ kJmol <sup>-1</sup>	$E(j) - E(i)^b$ (arbitr.units)	$F(i, j)^c$ (arbitr.units)
$\pi$ C1-C2	1.7241	$\pi^*$ C3-C4	0.3756	17.59	0.31	0.067
		$\pi^*$ C5-C6	0.3754	17.90	0.30	0.067
$\pi$ C3-C4	1.6603	$\pi^*$ C1C2	0.3467	18.72	0.28	0.065
		$\pi^*$ C5-C6	0.3754	18.52	0.28	0.065
		$\pi^*$ C20-C22	0.1243	17.41	0.30	0.068
C5-C6	1.6882	$\pi^*$ C1-C2	0.3467	17.46	0.30	0.065
		$\pi^*$ C3-C4	0.3756	19.59	0.31	0.070
$\pi$ C28-C29	1.6745	$\pi^*$ C26-C27	0.3616	19.12	0.31	0.069
$\pi$ C30-C31	1.6530	$\pi^*$ C26-C27	0.3616	19.34	0.29	0.067
		$\pi^*$ C28-C29	0.3795	22.93	0.27	0.071
LP(1) O7	1.9644	$\sigma^*$ C1-C2	0.0234	7.26	1.13	0.081
LP(2)O7	1.8421	$\pi^*$ C1-C2	0.0234	30.60	0.34	0.096
LP(2) O15	1.8294	$\pi^*$ C5-C6	0.3754	31.54	0.34	0.098
LP(2)O25	1.8885	$\sigma^*$ C20-H21	0.0189	0.52	0.74	0.018
		$\sigma^*$ C24-C26	0.0639	19.29	0.70	0.105
$\pi^*$ C5-C6	0.3754	$\pi^*$ C3-C4	0.3756	256.67	0.01	0.081
$\pi^*$ C24-O25	0.2141	$\pi^*$ C20-C22	0.1243	43.76	0.03	0.072
$\pi^*$ C28-C29	0.3795	$\sigma^*$ C26-C27	0.0234	196.48	0.02	0.085
		$\sigma^*$ C30-C31	0.2856	139.99	0.02	0.081

subject to NBO analysis is formed by the orbital overlap between LP (O) and  $\sigma^*$  (CH). Stabilization of  $E(2)$  related to  $n2$  (O25)  $\rightarrow \sigma^*$  (C20-H21) interactions is 0.52 kJmol<sup>-1</sup>, which shows the possibility of weak intra molecular hydrogen bonding. Because of rehybridization, the C-H bond distance is strengthened, shortened and blue shifted in the stretching wavenumber. The investigation shows that charge transfer occurs from lone pairs  $n$  (O7) and  $n$  (O15) of the methoxy oxygen atom to the  $\pi$  orbitals of phenyl ring ph1 with interaction energy 30.60 and 31.54 kJ/mol, respectively (44). Also about Mitotane, NBO analysis creates a new kind of conjugative interaction which causes stabilization energy. This interaction exists in the nature of molecule (46). A combined molecular orbital coefficient analysis and molecular orbital plots for ethyl 2-cyano-3-[5-(hydrazinooxalyl-hydrazonomethyl)-1H-pyrrol-2-yl]-acrylate, suggest that the nature of electronic excitations is  $\pi \rightarrow \pi^*$  while showing NBO analysis the presence of various intra and inter molecular interactions and hydrogen bonding in dimer and their corresponding second order stabilization energy  $E(2)$  (52). The second order perturbation theory analysis of Fock matrix in NBO basis is shown in Table 3 (44).

#### Mulliken population analysis: Mulliken atomic charge

The calculation of Mulliken atomic charge has an important role in the application of quantum chemical calculation in molecular system. Atomic charges influence dipole moment polarizability, electronic structure and more properties of molecular systems. The total atomic charges of DBHQ and DCHQ resulted from

Mulliken population analysis with 6-311++G (d,p) basis set. Based on the result, it is clear that the substitutions of Br, Cl and OH atoms in the heteroaromatic ring leads to redistribution of electron density. For DBHQ and DCHQ the Mulliken atomic charge has shown two C atoms occupies the higher positive values and gets more acidic and some C and H atoms takes the place of the low positive values and becomes less acidic. In halogen group the Mulliken atomic charges differ from negative to positive values, which causes an increase in electronegativity (Cl>Br) (43). The Mulliken charge distributions of rosmarinic acid have been done by DFT calculations. Among the group of oxygen atoms, the carboxylic group oxygen has the bigger negative charges compared with all other atoms of the molecules (45).

#### Molecular electrostatic potential

Molecular electrostatic potential (MEP),  $V(r)$  at a point  $r$  due to a molecular system with nuclear charges  $Z_A$  located  $R_A$  an electron density  $\rho(r)$  is given by

$$V(r) = \sum_{A=1}^N \frac{Z_A}{|r - R_A|} - \int \frac{\rho(r') d^3 r'}{|r - r'|} \quad (3)$$

The graphical representation of the molecular electrostatic potential surface (MEP), as described by Kollman and Singh is a series of values showing the evaluation of the interaction energy between a positively charged (proton) probe and points on solvent accessible surface as defined by Connolly. Areas of high electron density with a strong attraction between the proton and

the points on the molecular surface, has the brightest red colour and those of the lowest electron density have deep blue to indigo colour showing the regions of maximum repulsion. The molecular electrostatic potential (MEP) at a point in the space around the molecule gives a sign of the net electrostatic effect produced at that point by the total charge distribution (electron+nuclei) of the molecule and correlates with dipole moment, electronegativity, partial charges and chemical reactivity of the molecule. It creates a visual method to find out the relative polarity of the molecule. An electron density isosurface mapped with electrostatic potential surface shows the size, shape, charge density and site of chemical reactivity of the molecules. The different values of the electrostatic potential at the surface have been shown by different colours; red is a sign of regions with most negative electrostatic potential, blue shows regions of most positive electrostatic potential and green is a sign of regions of zero potential. The potential increases in the order red<orange<yellow<green<blue. Mapped molecular electrostatic on the  $\rho(r) = 0.0004$  a.u. isodensity surface for DMBC calculated at the B3LYP/6-311++G (d,p) level of theory is shown in Figure 4(a). This figure offers a visual representation of the chemically active site and relative reactivity at atoms.  $\pi$  – system of benzene rings posses a region of zero potential, leaving a more electrophilic region in the plane of hydrogen atoms. The shape of the electrostatic potential surfaces at sites near the polar carbonyl group in the molecule and the methoxy group is affected stereo structure and the charge density distribution. These sites indicate regions of the most negative electrostatic potential and high activity of the carbonyl group. In contrast, regions near the other two polar atoms – bromine and oxygen of methoxy groups – show regions where there is mildly negative potential. Figure 4(b) suggests the

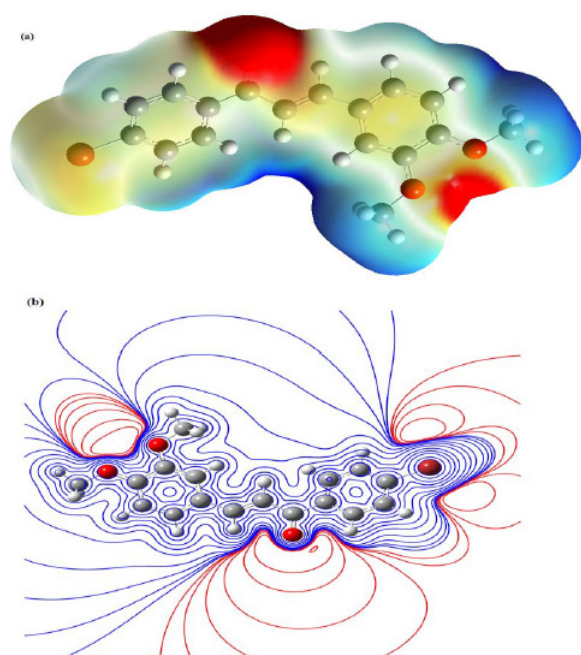


**Figure 4.** (a) Molecular electrostatic potential mapped on the  $\rho(r) = 0.0004$  a.u. isodensity surface in the range from  $-2.261E-2$  (Red) to  $+2.261E-2$  (Blue) for DMBC (b) Contour diagram calculated at the B3LYP/6-311++G (d,p) level of theory for DMBC (44).

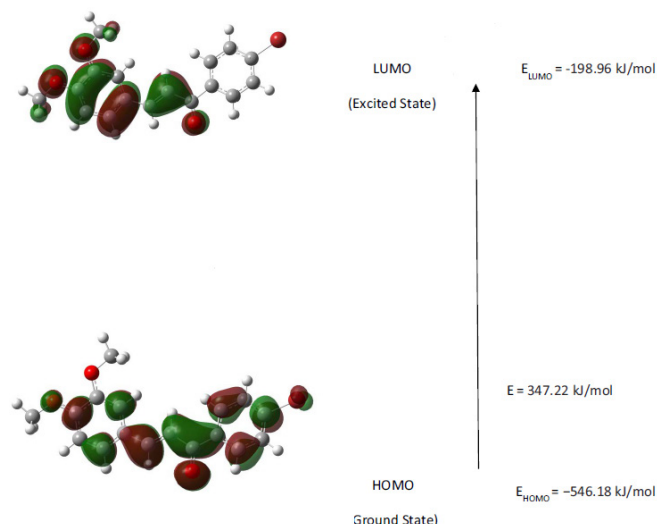


**Figure 5.** HOMO-LUMO plot by B3LYP/6-31G (d,p) level of theory for DMBC (44).

2-Dimensional projection of the map into the molecular plane (44). Potential of molecular electrostatic has also been used for DBHQ, DCHQ and rosmarinic acid (43, 45).

### HOMO-LUMO energy gap

The frontier molecular orbital play a significant role in the electric and optical properties and in uv-visible spectra and chemical reactions too (45). HOMO shows the ability to donate an electron, while, LUMO as an electron acceptor, shows the ability for obtaining an electron. Energy difference between HOMO and LUMO orbitals is named energy gap, which is important stability reflector for structures. A low HOMO-LUMO gap suggests lower stability of the molecule in the sense of its higher charge transfer in compounds. The conjugated molecules are featured by a small HOMO-LUMO separation, which is the result of a significant degree of ICT (intra molecular charge transfer) from the groups of electron donor to the efficient groups of electron acceptor through  $\pi$  conjugated path. For DMBC, the HOMO and LUMO energies at the DFT level,  $-546.18$  kJ/mol and  $-198.96$  kJ/mol, the energy gap equivalent to  $347.22$  kJ/mol shows the lowering of energy gap (Figure 5) (44). The atomic orbital compound and energy level of HOMO and LUMO orbitals have been calculated for rosmarinic acid. The analysis of the wave function show that the electron absorption conforms to the transition from the ground to the first excited states, mainly described by one-electron excitation from HOMO to LUMO. The HOMO and LUMO energies are  $-533.19$  kJ/mol and  $-173.29$  kJ/mol and the gap is  $359.9$  kJ/mol (45). Moreover, SCF energy for DBHQ and DCHQ is lower in the HOMO-LUMO energy gap (43). The lowering energy gap of HOMO-LUMO state the eventual charge transfer interaction happens, causing the biological activity of the molecule to increase.

### Molecular polarizability

One of the other investigations is studying the effect of basis set on molecular polarizability. Calculations of the molecular polarizability for anticancer medicines have been reported.  $\alpha$  is a second-rank tensor property called the dipole polarizability and mean polarizability  $\langle \alpha \rangle$  is assessed using the following equation (43).

$$\langle \alpha \rangle = 1/3(\alpha_{xx} + \alpha_{yy} + \alpha_{zz}) \quad (7)$$

### Thermodynamic properties

Several thermodynamic parameters and dipole moment have been calculated for anticancer drugs. The self consistent field (SCF) energy, zero point vibrational energies (ZPVE), rotational constant and entropy  $S_{vib}(T)$  have been calculated to the point of accuracy and variations in the ZPVEs appear to be in significant. In addition, total energies and enthalpy, Gibbs free energy and heat capacity have been obtained. The results show that the more electronegativity rises, the more total energies and enthalpy increase (Cl>Br). The increase of dipole moment can be due to hyper conjugative structures, thereby shortening the bond lengths. Lone pair electrons over N,O and halogen atoms make a noticeable contribution to the dipole moment of the molecules. It is scale of the asymmetry in the molecular charge distribution which is given as a vector in 3-dimensions. Thus, it can be used as a descriptor to depict the charge movement across the molecule. The direction of the dipole moment vector in a molecule relies on the center of positive and negative charges. Dipole moments are determined strictly for neutral molecules. For charged systems, the value of dipole moment vector depends on choosing the original orientation of the molecule (43,49,52).

### Conclusion

During the past years, the rapid advances in computational chemistry have resulted in increasingly accurate description of *anticancer* medicines. The accessibility of DFT and its TD formalism has made this technique an valuable tool to non- expert to describe and interpret key experimental properties of these medicines. Numerous functionals, Basis sets and corrections have been suggested, which are often optimized to create a specific property with high accuracy. As such, nuclear geometries are generally reproduced with satisfaction, while, the calculation of NMR chemical shifts requires larger basis sets for good accuracy. Although the quest of finding a universal functional is a prevailing challenge, DFT is steel a method to be chosen for a large number of theoretical analyses of anticancer drugs because it can provide a number of reasonable descriptors which aid to rational design.

Overall, this review provide key information about anticancer drugs, which is summarized as follows: Density functional theory calculations at the B3LYP/6-31G (d, p) and 6-311++G\*\* levels has been used to determine the ground state molecular geometry (bond lengths and bond angles), harmonic vibrational wavenumbers, infrared intensities and Raman activities of anticancer drugs. The wavenumbers have been shown very good agreement with the experimentally determined values. A comparison of the theoretical spectra and experimental FT-IR and FT-Raman spectra of these molecules has been made and complete vibrational assignments of the experimental spectra have been proposed. NBO analysis creates an efficient method for investigation inter and intra molecular interaction in molecular system. The stabilization energy has been computed from second order perturbation theory. The NBO analysis

has been cleared that the  $\pi \rightarrow \pi^*$  interaction gives the strongest stabilization to the system. The NBO, electrostatic potential map analysis and the HOMO and LUMO analysis, reveal the significant degree of charge transfer interactions happening in the molecules, which is responsible for bioactive property of the biomedical compounds.

### References

1. Sharifi-Rad, J., Sharifi-Rad, M., Hoseini-Alfatemi, S.M., Iriti, M., Sharifi-Rad, M. and Sharifi-Rad, M., Composition, Cytotoxic and Antimicrobial Activities of *Satureja intermedia* C.A.Mey Essential Oil. *Int. J. Mol. Sci.* 2015, **16**(8):17812-17825. doi: org/10.3390/ijms160817812.
2. Sharifi-Rad, J., Hoseini-Alfatemi, S.M., Sharifi-Rad, M., Sharifi-Rad, M., Iriti, M., Sharifi-Rad, M., Sharifi-Rad, R. and Raiesi, S., Phytochemical Compositions and Biological Activities of Essential Oil from *Xanthium strumarium* L.. *Molecules* 2015, **20**(4):7034-7047. doi: org/10.3390/molecules20047034.
3. Sharifi-Rad, J., Miri, A., Hoseini-Alfatemi, S.M., Sharifi-Rad, M., Setzer, W.N., Hadjiakhoondi, A., Chemical Composition and Biological Activity of *Pulicaria vulgaris* Essential Oil from Iran. *Nat. Prod. Commun.* 2014, **9**(11):1633-1636.
4. Yadav, A. and Singh, V.K., The antineoplastic behaviour of nitrosoureas: an ab initio study. *J. Molecular Struct.* 1997, **389**:191-198. doi: org/10.1016/S0166-1280(96)04638-6.
5. Sen, F., Ekici, O., Dincer, M. and Cukurovali, A., A comparative study on 4-(4-(3-mesityl-3-methylcyclobutyl)thiazole-2-yl)-1-thia-4-azaspiro[4.5] decan-3-one: Experimental and density functional methods. *J. Molecular Struct.* 2015, **1086**:109-117. doi: org/10.1016/j.molstruc.2014.12.088.
6. Soltani, A., Baei, M.T., Ghasemi, A.S., Lemeski, E.T. and Amirabadi, K.H., Adsorption of cyanogen chloride over Al- and Ga-doped BN nanotubes. *Superlattice Microst.* 2014, **75**:564-575. doi: org/10.1016/j.spmi.2014.07.033.
7. Ghasemi, A.S., Molla, M. and Ashrafi, F., Study of Nuclear Qua drupole Resonance on CO-doped Single-Walled Carbon Nanotubes: A DFT Computation. *Res. J. Appl. Sci. Eng. Technol.* 2012, **4**(15):2543-2547. doi: org/10.1098/rsta.2010.0111.
8. Ghasemi, A.S. and Molla, M., Highly Sensitive Single-Walled Carbon Nanotube (5,0) for Adsorptions Gases CO<sub>2</sub>, CO and N<sub>2</sub> : A DFT Study. *Int. J. Chem.Tech. Res.* 2012, **4**:1302-1308.
9. Ghsemi, A.S. and Ashrafi, F., Density Functional Theory (DFT) Study of O<sub>2</sub>, N<sub>2</sub> Adsorptions on H-Capped (4,4) Single-Walled Carbon Nanotube. *Res. J. Appl. Sci. Eng. Technol.* 2012, **4**(15):2523-2528. doi: 10.1155/2012/819490
10. Ashrafi, F., Ghasemi, A.S., Babanejad S.A. and Rahimof, M., Optimization of Carbon Nanotubes for Nitrogen Gas Adsorption, *Res. J. Appl. Sci. Eng. Technol.* 2010, **2**(6):547-551.
11. Ashrafi, F. and Ghasemi, A.S., Density Functional Theory (DFT) Study of O<sub>2</sub>, N<sub>2</sub> Adsorptions on H-Capped (5, 0) Single-Walled Carbon Nanotube (CNT). *E- J. Chem.* 2012, **9**(4):2134-2140.
12. Babanejad, S.A. Ashrafi, F. and Ghasemi, A.S., Optimization of Adsorption of Oxygen Gas on Carbon Nanotubes Surface. *Arch. Appl. Sci. Res.* 2010, **2**(5):438-443.
13. Ghasemi, A.S. and Ashrafi, F., Babanejad, S. A. and Rahimof, M. A Computational NMR Study of Chemisorption of Nitrogen-Doped on the Surface of Single-Walled Carbon Nanotubes. *Arch. Appl. Sci. Res.* 2010, **2**(4):262-270.
14. Ghasemi, A.S. and Ashrafi, F.A., Computational NMR Study for Chemisorption of Oxygen-doped on the Surface of Single-walled Carbon Nanotubes. *Res. J. Appl. Sci. Eng. Tech.* 2012, **4**(15):2529-2536.

15. Babanegad, S.A., Ashrafi, F., Ghasemi, A.S. and Ashrafi, E., Influence of Hydrogen Doping on the <sup>15</sup>N and <sup>17</sup>O NMR Arameters in Zigzag and Armchair Single Wall Nanotube: A DFT Study. *Der. Chem. Sin.* 2012, **3**(1):124-128.
16. Ghasemi, A.S. and Aashrafi, F., Adsorption <sup>17</sup>O, <sup>15</sup>N and CO Molecules on the Surface of SWCNT: A Computational NMR Study, *Int. J. ChemTech Res.* 2012, **4**:1295-1301.
17. Ghasemi, A.S., Rezaei, M. and Molla, M., Density Functional Theory (DFT) Study Adsorptions On Single-Walled Carbon Nano Tube-A Review. *Int. J. ChemTech Res.* 2013, **5**:1585-1593.
18. Ashrafi, F., Babanegad, S.A. and Ghasemi, A.S., Comparison of Adsorption of Nitrogen and Oxygen- Molecules on the Open Ended and Surface of Swcnts: A Computational NMR and NQR Study. *Res. J. Appl. Sci. Eng. Tech.* 2012, **4**(7):795-801.
19. Ghasemi, A.S., A DFT Computation for Compaison of NQR of O<sub>2</sub>, N<sub>2</sub> and CO over the Surface of Single-Walled Carbon Nanotubes. *Res. J. Appl. Sci. Eng. Tech.* 2013, **5**(6):1892-1898.
20. Ghasemi, A.S., Molla, M. and Mostashregh, M., Adsorptions Gas CO<sub>2</sub> on the Surface and Open-Ended Single-Walled Carbon Nanotube: A NQR Study. *Int. J. ChemTech Res.* 2013, **5**:1623-1629.
21. Mircescu, N.E., Varvescu, A., Herman, K., Vasile, C. and Nicolae, L., Surface-Enhanced Raman and DFT Study on Zidovudine. *Spectroscopy.* 2011, **26**(4-5):311-315. doi: org/10.1155/2011/401828.
22. Gökalp, F., A Theoretical Study of Curcuma Longa's Anticancer Agents, Curcumin I and Curcumin II, in Blood and Gas by Using Density Functional Theory (DFT) and Hartree-Fock (HF). *Int. J. Medicine and Medical Sci.* 2014, **6**:146-150.
23. Ghahremani, H., Bagheri, S. and Hassani, S.M., Theoretical study on physicochemical and geometrical properties of the adriamycin conjugated gold nanoparticles. *Int. J. Pharmacy and Pharmaceutical Sci.* 2012, **4**:751-754.
24. Ghahremani, H. and Hassani, S.M., A Study on the Geometrical and Physicochemical Properties of Daidzein-Daunomycin Conjugate Using Density Functional Theory and Hartree-Fock. *Int. J. PharmTech Res.* 2012, **4**:130-134.
25. Hassani, S.M. and Bagheri, S., Theoretical Study on Physicochemical and Geometrical Properties of Doxorubicin-PEG-FOL Nanoparticles and Daunorubicin-PEG-FOL Nanoparticles. *Adv. Biores.* 2012, **3**: 45-48.
26. Hassani, S.M. and Bagheri, S., Computational Procedure for Determining Physicochemical Properties of Doxorubicin- PLGA Nanoparticles and Daunorubicin-PLGA Nanoparticles. *Int. J. Pharm. Tech. Res.* 2012, **4**:1242-1246.
27. Hassani, S.M., Ghahremani, H. and Bagheri, S., The Estimation of the Solubility of Daidzein- Adriamycin conjugate and Adriamycin Based on Density Functional Theory and Hartree-Fock studies. *Arch. Appl. Sci. Res.* 2011, **3**:296-300.
28. Bagheri, S., Chamani, Z. and Hassani, S.M., A Computational Study on the PhysicoChemical and Geometrical Properties of Daunorubicin-GA3, Daunorubicin-M GA3, DOX-GA3 and DOX-MGA3. *Int. J. Chem. Tech. Res.* 2012, **4**:63-67.
29. Rahimi, F., Bahlake, A., Chamani, Z. and Bagheri, S., Theoretical Study on the Conjugation of PLGA and PLGA-PEG Carriers to Doxorubicin and Daunorubicin. *Eur. J. Exp. Bio.* 2012, **2**:2055-2060.
30. Liao, J., Zhao, H. and Zhou, L., Theoretical Study on the Bi-functional Substitution Reactions Between Gold(III) Dithiocarbamate Derivative Au(DMDT)Cl<sub>2</sub>(DMDT = N,N-DimethylDithio-Carbamate) and Target Molecules. *Comput. Theore. Chem.* 2014, **1048**:84-94. doi: org/10.1016/j.comptc.2014.08.027.
31. Sarmah, P. and Deka, R.C., Hydrolysis and Binding Mechanism of AMD473 (cis-[PtCl<sub>2</sub>(NH<sub>3</sub>)(2-Picoline)]) with Guanine: a Quantum Mechanical Study. *J. Mol. Str.: THE.* 2010, **955**:53-60. doi: org/10.1016/j.theochem.2010.05.030.
32. Shishkin, O.V., Pelmenschikov, A., Hovorun, D.M. and Leszczynski, J., Free Canonical 2'-Deoxyribonucleosides: A Density Functional Study. *J. Mol. Str.* 2000, **526**:329-341. doi: org/10.1016/S0022-2860(00)00497-X.
33. Jäger, M., Freitag, L. and González, L., Using Computational Chemistry to Design Ru Photosensitizers with Directional Charge Transfer. *Coord. Chem. Rev.* 2015, **304-305**: 146-165. doi: org/10.1016/j.ccr.2015.03.019.
34. Vlček, J.A. and Zálíš, S., Modeling of Charge-Transfer Transitions and Excited States in d<sup>6</sup> Transition Metal Complexes by DFT Techniques. *Coord. Chem. Rev.* 2007, **251**:258-287. doi: org/10.1016/j.ccr.2006.05.021.
35. Neese, F., Prediction of molecular properties and molecular spectroscopy with density functional theory: From fundamental theory to exchange-coupling. *Coord. Chem. Rev.* 2009, **253**:526-563. doi: org/10.1016/j.ccr.2008.05.014.
36. Koch, W. and Holthausen, M.C.A., Chemist's Guide to Density Functional Theory, *Wiley-VCH*, 2000, ISBNs: 3-527-30372-3 (Softcover); 3-527-60004-3 (Electronic)
37. Chermette, H. Density Functional Theory: A Powerful Tool for Theoretical Studies in Coordination Chemistry. *Coord. Chem. Rev* 1998, **178-180**:699-721. doi: org/10.1016/S0010-8545(98)00179-9.
38. Dreuw, A. and Head-Gordon M., Single-Reference ab Initio Methods for the Calculation of Excited States of Large Molecules. *Chem. Rev.* 2005, **105**:4009-4037. doi: org/10.1021/cr0505627.
39. Tshipis, A.C., DFT Flavor of Coordination Chemistry. *Coord. Chem. Rev.* 2014, **272**:1-29. doi: org/10.1016/j.ccr.2014.02.023.
40. Kohanoff, J. and Gidopoulos, N.I., Density Functional Theory: Basics, New Trends and Applications. *Handbook of Mol. Phys. Quan. Chem.* 2003, **2**:532-568.
41. Casida, M.E. Time-Dependent Density-Functional Theory for Molecules and Molecular Solids. *J. Mol. Struct.: THEOCHEM*, 2009, **914**:3-18. doi: org/10.1016/j.theochem.2009.08.018.
42. Casida, M.E. and Huix-Rotllant, M., Progress in Time-Dependent Density-Functional Theory. *Annual Rev. Phys. Chem.* 2012, **63**:287-323. doi: org/10.1146/annurev-physchem-032511-143803.
43. Lakshmi, A., Balachandran, V. and Janak, A., Comparative Vibrational Spectroscopic Studies, HOMO-LUMO and NBO Analysis of 5,7-Dibromo-8-Hydroxyquinoline and 5,7-Dichloro-8-Hydroxyquinoline Based on Density Functional Theory, *J. Mol. Stru.* 2011, **1004**:51-66. doi: org/10.1016/j.molstruc.2011.07.022.
44. Joseph, L., Arunsasi, B.S., Sajan, D. and Shettigar, V., Synthesis, Crystal Growth, Thermal, Electronic and Vibrational Spectral Studies of 1-(4-Bromophenyl)-3-(3, 4-Dimethoxy-phenyl) Prop-2-en-1-one: A Density Functional Theory Study. *J. Mol. Str.* 2014, **1076**:687-697. doi: org/10.1016/j.molstruc.2014.08.008.
45. Mariappan, G., Sundaraganesan, N. and Manoharan, S., Experimental, and Theoretical Spectroscopic Studies of Anticancer Drug Rosmarinic Acid Using HF and Density Functional Theory. *Spectrochimica Acta Part A: Mol. Bio. Spect.* 2012, **97**:340-351. doi: org/10.1016/j.saa.2012.06.011.
46. Mariappan, G. and Sundaraganesan, N., Structural and Vibrational Spectroscopic Analysis of Anticancer Drug Mitotane Using DFT Method; A Comparative Study of its Parent Structure. *J. Mol. Stru.* 2015, **1086**:73-85. doi: org/10.1016/j.molstruc.2014.12.063.
47. Sharifi-Rad, J., Hoseini-Alfatemi, S.M., Sharifi-Rad, M. and Teixeira da Silva, J.A., Antibacterial, Antioxidant, Antifungal and Anti-Inflammatory Activities of Crude Extract from *Nitraria Schoberi* Fruits. *Biotech*, 2015, **5**(5):677-684. doi: org/10.1007/s13205-014-0266-1.
48. Sadasivam, K. and Kumaresan, R., Theoretical Investigation on the Antioxidant Behavior of Chrysoeriol and Hispidulin Flavonoid Compound -A DFT Study. *Compu. Theor. Chem.* 2011, **963**: 227-235. doi: org/10.1016/j.comptc.2010.10.025.

49. Sharma, A.V. Gupta, R., Mishra, P.T., Maeda, S. and Kunimoto, K.K., Study of Vibrational Spectra and Molecular Structure of Inter-Molecular Hydrogen Bonded 2-Thiohydantoin Using Density Functional Theory. *J. Mol. Struc.* 2011, **1004**:237–247, doi: org/10.1016/j.molstruc.2011.08.011.

50. Singh, R.N., Kumar, A., Tiwari, R.K., Rawat, P., Verma, D. and Baboo, V., Synthesis Molecular Structure and Spectral Analysis of Ethyl 4-Formyl-3,5-Dimethyl 1H-Pyrrole-2-Carboxylate Thiosemicarbazone: A Combined DFT and AIM Approach. *J. Mol. Struc.* 2012, **1016**:97–108. doi: org/10.1016/j.molstruc.2012.02.033.

51. Pulay, P., Fogarasi, G., Pong, F. and Boggs, J.E., Systematic

Ab initio Gradient Calculation of Molecular Geometries, Force Constants and Dipole-Moment Derivatives. *J. Am. Chem. Soc.* 1979, **101**:2550–2560. doi: org/10.1021/ja00504a009.

52. Singh, R.N., Kumar, A., Tiwari, R.K. and Rawat P., Synthesis molecular structure, multiple interactions and chemical reactivity analysis of a novel ethyl 2-cyano-3-[5-(hydrazinooxalyl-hydrazonomethyl)-1H-pyrrol-2-yl]-acrylate and its dimer: A combined experimental and theoretical (DFT and QTAIM) approach. *J. Mol. Struct.* 2013, **1037**:420–430. doi: org/10.1016/j.molstruc.2013.01.011